drones

*Article*

# A Modified Model-Free Adaptive Control Method for Large-Scale Morphing Unmanned Vehicles

**Haohui Che [1], Jun Chen [2], Guanghui Bai [3] and Jianying Wang [1,*]**

[1] School of Aeronautics and Astronautics, Sun Yat-Sen University, Shenzhen 518107, China
[2] China Academy of Launch Vehicle Technology, Beijing 100076, China; chenjun1969119@163.com
[3] Science and Technology on Space Physics Laboratory, Beijing 100076, China; baigh2019@163.com
* Correspondence: wangjiany@mail.sysu.edu.cn

**Abstract:** This paper investigates the attitude control problem for large-scale morphing unmanned vehicles. Considering the rapid time-varying and strong aerodynamic interference caused by large-scale morphing, a modified model-free control method utilizing only the system input and output is proposed. Firstly, a two-loop equivalent data model for the morphing unmanned vehicle is developed, which can better reflect the practical dynamics of morphing unmanned vehicles compared to the traditional compact form dynamic linearization data model. Based on the proposed data model, a modified model-free adaptive control (MMFAC) scheme is proposed, consisting of an external-loop and an inner-loop controller, so as to generate the required combined control torques. Additionally, in light of the aerodynamic uncertainties of the large-scale morphing unmanned vehicle, a rudder deflection actuator control scheme is designed by employing the model-free adaptive control approach. Finally, the boundedness of the closed-loop system and the convergence of tracking errors are guaranteed, based on the stability analysis. Additionally, numerical examples are presented to demonstrate the effectiveness and robustness of the proposed control scheme in the case of the effect of large-scale morphing.

**Keywords:** attitude control; morphing vehicle; model-free adaptive control



**Citation:** Che, H.; Chen, J.; Bai, G.; Wang, J. A Modified Model-Free Adaptive Control Method for Large-Scale Morphing Unmanned Vehicles. *Drones* **2023**, *7*, 495. https://doi.org/10.3390/drones7080495

Academic Editors: Kai Liu, Yongji Wang, Jia Song and Lei Liu

Received: 3 July 2023
Revised: 22 July 2023
Accepted: 25 July 2023
Published: 27 July 2023



## 1. Introduction

Recent years have witnessed the vigorous development of morphing unmanned vehicles due to the advances in smart technologies, including structures, materials, sensors, and actuators [1–3]. Typically, the concept of a morphing unmanned vehicle refers to the unmanned vehicle with large scale shape changes or transfigurations [4–6]. Compared to fixed-wing vehicles, the morphing vehicle can change its configuration to achieve optimal performance under multiple flight conditions, making it possible to fly in a wider space/velocity envelope with greater maneuverability [7]. However, the strong time-varying, nonlinear dynamic characteristics, and aerodynamic interferences during morphing cause the attitude stabilization and control for morphing vehicles to become key problems and impose significant challenges. Many experts and scholars are committed to related studies and have made important progress in these areas [8–10].

The fast time-varying and strong aerodynamic interference caused by large scale morphing suggest the requirements for controller design, and the adaptive and robust requirements are becoming higher [11]. With respect to the uncertainties and disturbances of the morphing process, robust control theories are widely used to improve the vigorous performance of the current control system. Dario et al. [12] investigated the flight control problem for a folding-wing vehicle subject to large-scale shape changes and proposed a multiloop controller based on the robust control reduction technique linear quadratic output feedback inner-loop controller and the linear parameter-varying outer-loop controller. The simulation results showed that the robust controller successfully maintained the stability

during morphing. Bao et al. [13] considered the integration of the guidance, control, and morphing problem for a morphing vehicle with variable span wing. An adaptive dynamic surface back-steeping control method with stability analysis was proposed to establish the integrated system and attenuate the uncertain dynamics resulting from morphing. Liu et al. [14] considered the trajectory tracking problem for the morphing vehicle in the presence of model uncertainties. A novel robust control framework, including an adaptive feedback control law and an adaptive control allocation law, was proposed to attenuate the uncertain dynamics resulting from the wing shape change. Yan et al. [15] established an explicit mathematical model of a wing-sweeping vehicle and designed a sliding mode controller based on the adaptive super-twisting theory. The simulation results verified the robustness of the proposed controller in the presence of disturbances during the morphing process. Seen from the aforementioned works, the nonlinear robust control algorithms can effectively improve the global stability and robustness of the system. However, it is noticed that most of the nonlinear control algorithms are presented based on the explicit and accurate nonlinear modeling of the morphing vehicle, which makes it more complex to design and calculate the nonlinear control system. Additionally, the upper bound of the model uncertainties and external disturbances are required for the robust nonlinear controller design [16,17]. However, in practical engineering applications, it becomes more difficult to obtain the accurate value of such an upper bound, due to the fast time-varying aerodynamic characteristics and the great differences between ground prediction and actual flight.

In this sense, data-driven control methods, which are designed by utilizing the input/output (I/O) data of the system instead of the precise information of the mathematical model [18], posess the inherent advantage of solving the above problems. Several popular data-driven methods, such as active disturbance rejection control (ADRC) [19,20], model-free adaptive control (MFAC) [21], and the balanced mode decomposition algorithm [22], have been applied to the morphing vehicles, showing satisfactory performance for the morphing vehicles with great model changes and model uncertainties. Among these methods, MFAC shows the advantage of effective control performance with a simple structure, and it is regarded as a preferred option for the control problem of complex nonlinear systems.

The essential idea behind MFAC is the establishment of a virtual equivalent data model for the discrete nodes to express the relationship between the output data and input data, updating the parameters of the data model using the online I/O data, and designing the adaptive control law based on the derived data model [23–25]. Through the efforts of many scholars, the MFAC method has been developed into a systematic and mature control theory which is applied in many practical fields [26–28]. However, the original MFAC algorithm, based on compact form dynamic linearization (CFDL) or partial form dynamic linearization (PFDL) technology, cannot be directly applied to the flight control problem of a vehicle, since the data models of CFDL and PFDL are not strictly applicable to vehicles dynamics. In order to solve this inapplicability problem, Qi et al. [21] proposed a novel controller cascading the PLDL-MFAC and a proportional-derivative (PD) controller for a very flexible vehicle and achieved greater effective and robust performance in the presence of uncertainties and disturbances. Che et al. [29] introduced the time series of historical output data errors into control law to increase the damping effects, achieving the convergence and stability analysis of the improved controller. From the above studies, it can be concluded that increasing the damping of the controller is a viable approach to solve the inapplicable problem. However, adding damping to the controller is a somewhat indirect approach and may result in slowing down the convergence speed. Therefore, a direct and more effective control approach is required to solve such a problem.

To this end, this paper develops a novel CFDL data model for the morphing unmanned vehicle, including an inner loop and an external loop, which can better reflect the dynamic characteristics of morphing vehicles. Then, a modified MFAC (MMFAC) scheme based on the proposed data model is proposed to achieve a more efficient tracking performance under fast time-varying and strong aerodynamic interference. Furthermore,

considering the unknown aerodynamic data of the controlled vehicle, a rudder actuator control scheme is designed using the CFDL-MFAC method. Finally, the stability analysis of the resulting control system is provided. Moreover, the effectiveness and advantages of the proposed control strategy are verified by numerical simulations for the large-scale morphing unmanned vehicles.

The remainder of this paper is organized as follows. Section 2 reviews basic MFAC control theories and formulates the data-driven attitude control problem for large-scale morphing unmanned vehicles. Section 3 proposes the modified model-free adaptive control method for large-scale morphing unmanned vehicles, including dynamic data modeling, the inner/external loop attitude control, and the actuator control strategy design; the boundedness of the closed-loop system and the convergence of tracking errors are also guaranteed based on the stability analysis. The simulations and results of the proposed controller are shown in Section 4, and conclusions are provided in Section 5.

## 2. Fundamental Knowledge and Problem Formulation

### 2.1. Definition of Coordinate System

In order to describe the position and attitude of the morphing vehicle, the reference coordination systems, notation, and orientation are defined in Figure 1 and Table 1. In the launching coordinate system, $\varphi$, $\psi$, and $\gamma$ describe the Euler attitude angle, representing the pitch angle, yaw angle, and roll angle, respectively. In the body-fixed coordinate system, $\omega_{x1}$, $\omega_{z1}$, and $\omega_{y1}$ are the angular velocity of the roll, pitch, and yaw angle, respectively.

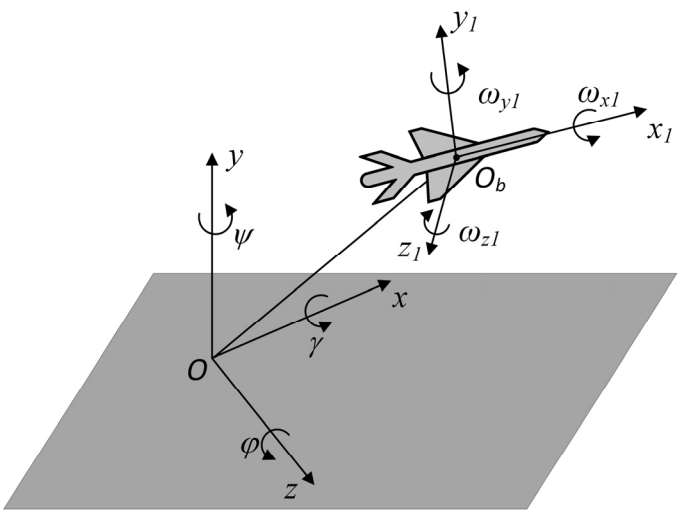


**Figure 1.** Reference coordinate systems of the unmanned vehicle.

**Table 1.** Notation and orientation of the reference coordinate systems.

| Coordinate | Notation | Orientation |
|---|---|---|
| Launching coordinate system $O-xyz$ | $O$ | Initial position of the vehicle |
| | $Ox$ | Pointing to the terminal position, parallel to the local geoid surface |
| | $Oy$ | Pointing upwards along the vertical plane |
| | $Oz$ | Forming a Cartesian right-hand system with $Ox$ and $Oy$ |

**Table 1.** *Cont.*

| Coordinate | Notation | Orientation |
| --- | --- | --- |
| Body-fixed coordinate system $O_b - x_1y_1z_1$ | $O_b$ | Center of gravity of the morphing vehicle |
| | $O_b$ | Pointing to the nose direction in the symmetry plane of the vehicle |
| | $O_bx_1$ | Pointing upwards in the symmetry plane of the vehicle, perpendicular to the $O_bx_b$ |
| | $O_by_1$ | Forming a Cartesian right-hand system with $O_bx_1$ and $O_by_1$ |

### *2.2. CFDL-MFAC Framework Formulation*

The nonlinear single-input and single-output (SISO) system is described as follows:

$$y(k+1) = f\big(y(k), \ldots, y\big(k-n_y\big), u(k), \ldots, u(k-n_u)\big) \tag{1}$$

where $y(k)$ and $u(k)$ are the output and input of the system, respectively, $n_u$ and $n_y$ are the unknown orders, and $f$ is an unknown nonlinear function.

**Assumption 1.** *The partial derivatives of $f$ with respect to the control input $u(k)$ is continuous.*

**Assumption 2.** *The change of the system output is bounded and satisfies $|\Delta y(k+1)| \leq \overline{\phi}|\Delta u(k)|$ with $\overline{\phi}$ being a positive constant.*

**Assumption 3.** *The sign of $\phi(k)$ remains unchanged at all times; $k$ , namely, $\phi_c(k) > \underline{\varepsilon} > 0$ or $\phi_c(k) < -\underline{\varepsilon}$, where $\underline{\varepsilon}$ is a small positive constant.*

**Remark 1.** *In practice, the above assumptions are deemed reasonable and acceptable. Assumption 1 is commonly employed in control system design for general nonlinear systems. It provides a practical and useful framework for modeling and analyzing complex nonlinear dynamic systems. Assumption 2 introduces an upper bound limitation on the change rate of the system output associated with a change in the control input. From the 'energy' standpoint, Assumption 2 can be interpreted to mean that the change rate of the system's energy is finite if the change in the control input energy is constrained within a finite altitude [23]. In Assumption 3, the sign of $\phi(k)$ plays a crucial role in determining the expected system output, which is similar to the concept of 'control direction' in the model-based control theory [29].*

Satisfying Assumptions 1~3, the nonlinear system can be equivalently expressed as the following CFDL data model [30]:

$$\Delta y(k+1) = \phi_c(k)\Delta u(k), \tag{2}$$

where $\phi_c(k)$ is a time-varying parameter called the pseudo-partial derivative (PPD).

Considering the control goal of tracking the desired signal with smooth control input, the control performance index is defined as

$$J_{u(k)} = |y^*(k+1) - y(k+1)|^2 + \lambda|u(k) - u(k-1)|^2, \tag{3}$$

where $y^*(k+1)$ is the desired output state, and $\lambda > 0$ is a weighting constant.

To estimate the time-varying PPD $\phi_c(k)$, the performance function for the unknown PPD estimation is given by

$$J_{\phi_c(k)} = \big|\Delta y(k) - \hat{\phi}_c(k)\Delta u(k-1)\big|^2 + \mu\big|\hat{\phi}_c(k) - \hat{\phi}_c(k-1)\big|^2. \tag{4}$$

By minimizing the cost functions (3) and (4) with respect to $u(k)$ and $\phi_c(k)$, respectively, one can obtain the MFAC scheme as follows:

$$\hat{\phi}_c(k) = \hat{\phi}_c(k-1) + \frac{\eta \Delta u(k-1)}{\mu + \Delta u(k-1)^2}(\Delta y(k) - \hat{\phi}_c(k-1)\Delta u(k-1)), \tag{5}$$

$$\hat{\phi}_c(k) = \hat{\phi}_c(1),\ if\ |\phi_c(k)| \leq \varepsilon\ or\ \text{sign}(\hat{\phi}_c(k)) \neq \text{sign}(\hat{\phi}_c(1)), \tag{6}$$

$$u(k) = u(k-1) + \frac{\rho \hat{\phi}_c(k)(y^*(k+1) - y(k))}{\lambda + |\hat{\phi}_c(k)|^2}, \tag{7}$$

where $\eta$ and $\rho$ are step factors with $\eta \in (0,1)$ and $\rho \in (0,1)$, and $\mu$ and $\lambda$ are penalty factors with $\mu > 0$ and $\lambda > 0$. Equation (6) is the reset rule of PPD estimation, which is used to facilitate the update of PPD.

### *2.3. PD-MFAC Algorithm Formulation*

Under Assumption 3 of the original CFDL-MFAC theory, the sign of PPD $\phi_c(k)$ is assumed to be unchanged. However, Assumption 3 is not feasible for the attitude control problem of vehicles. For instance, for vehicles, when the time derivative of the $y(k)$ is negative, the value of $y(k)$ would decrease, whether $\Delta u(k)$ is positive or negative, where $y(k)$ represents the attitude Euler angles, and $u(k)$ represents the control torques. In this regard, to ensure that the dynamic linear data model holds, the sign of the PPD parameter must be opposite to the sign of the control input, while the time derivative of $y(k)$ is less than zero, which is contrary to Assumption 3 that the sign of PPD remains unchanged. Similarly, Assumption 3 is not satisfying while the time derivative of $y(k)$ is positive. Therefore, the original CFDL data model cannot be directly employed to design the vehicle controller for the attitude control problem.

Without modifying Assumption 3, introducing an extra damping effect into the data model is a preferred approach to accommodate the MFAC method in the control problem of vehicles. For instance, in Ref. [21], a proportional-derivative term including the derivative of the system output is incorporated into the data model to obtain an appropriate dynamic response as follows.

$$\Delta y(k+1) = \xi(k)\Delta u(k) + |\xi(k)|(K_y \Delta y(k) + K_{dy}\frac{\Delta y(k) - \Delta y(k-1)}{T}) \tag{8}$$

where $K_y > 0$, $K_{dy} > 0$, and $T$ is the sample time.

Similar to the design process of the CFDL-MFAC controller, by minimizing the cost function (3) and introducing the step parameters, the PD-MFAC method proposed in Ref. [21] is obtained:

$$\hat{\xi}(k) = \hat{\xi}(k-1) + \frac{\eta_1 \Delta u(k-1)\left(\Delta y(k) - \hat{\xi}(k-1)\Delta u(k-1)\right)}{\mu_1 + |\Delta u(k-1)|^2} \tag{9}$$

$$\Delta u(k) = \frac{\rho \hat{\xi}(k)(y_r(k+1) - y(k))}{\lambda_1 + |\hat{\xi}(k)|^2} - sign(\hat{\xi}(k))(K_y \Delta y(k) + K_{dy}\frac{\Delta y(k) - \Delta y(k-1)}{T}) \tag{10}$$

It is noted that the PD-MFAC algorithm would be defined as a baseline controller for comparison in the simulation to verify the effectiveness of the proposed control scheme.

### *2.4. Problem Formulation*

A data-driven attitude control scheme for the large-scale morphing unmanned vehicle is considered in this study. When the vehicle is subjected to large deformations in flight, unmodeled dynamics and unpredictable model uncertainties are inevitable, which would

limit the performance of model-based control methods. In order to solve this problem, this paper aims to design attitude control laws for morphing unmanned vehicles using model-free adaptive control theories, such that the morphing vehicles is able to track the reference attitude angles and maintain stability in the absence of establishing mathematical models.

## 3. Modified Model-Free Adaptive Control Scheme Design

### *3.1. The Framework of the Control System*

The control system is divided into the attitude control and actuator control, as shown in Figure 2. In the attitude control design, a novel data model of the attitude dynamics of morphing vehicles is presented, and a two-loop controller scheme is proposed to achieve attitude tracking. For the external loop, the controller's purpose is to track the reference attitude and generate an attitude angular velocity command for the inner loop. For the inner loop, the controller not only tracks the attitude angular velocity command from the external loop, but also tracks the reference attitude angular velocity. To facilitate the whole control process, the actuator control strategy using the MFAC algorithm is proposed to track the control torque command from the attitude controller.

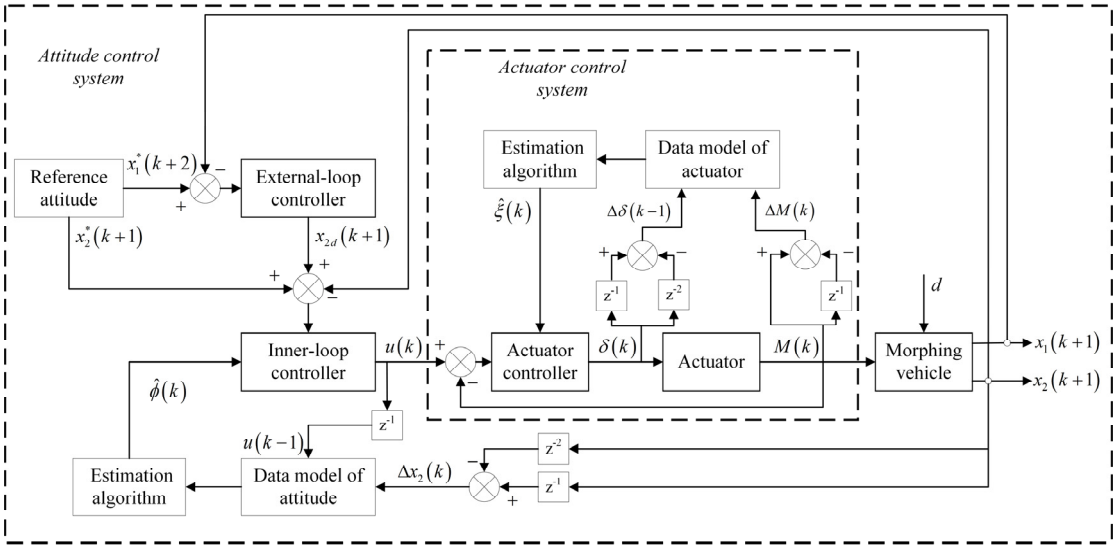


**Figure 2.** The control block diagram of the model-free attitude control system.

#### 3.1.1. MMFAC Attitude Controller Design

Under the assumption of small angles, the attitude dynamic equation of the vehicle in the pitch channel can be presented as Equation (11), where the attitude coupling and external disturbances are not considered [31]. It is worth pointing out that the following model is only used to clearly realize the essential dynamics of the vehicles, but not to describe the accurate dynamics model.

$$\begin{cases} \dot{\varphi} = \omega_{z1} \\ \dot{\omega}_{z1} = \frac{1}{I_Z} M_Z \end{cases} \tag{11}$$

where $I_Z$ is the rotational inertia of the $O_b z_1$ axis, and $M_Z$ is the control torque of $O_b z_1$ axis.

From Equation (11), it can be found that the second derivative of attitude angle is linearly related to the control torque. By introducing the PPD parameter $\overline{\phi}(t)$, the vehicle data model can be modified as follows:

$$\begin{cases} \dot{x}_1 = x_2 \\ \dot{x}_2 = \overline{\phi}(t) u \end{cases} \tag{12}$$

where $x_1$ represents the attitude angle, $x_2$ represents the attitude angle velocity, and $u$ is control torque.

By discretizing Equation (12), one can obtain the following modified data model:

$$\begin{cases} x_1(k+1) = x_1(k) + Tx_2(k) \\ x_2(k+1) = x_2(k) + \phi(k)u(k) \end{cases} \tag{13}$$

where $T$ is the sampling time and $\phi(k) = T\overline{\phi}(t)$.

Comparing Equation (11) with Equation (13), the value of $\phi(k)$ is equal to $T/I_Z$, where the rotational inertia $I_Z$ of the morphing vehicle is positive and bounded. Thus, it can be concluded that the PPD $\phi(k)$ is a constant positive and bounded parameter, namely,

$$0 < \phi(k) \leq b. \tag{14}$$

Employing the data models Equation (13), the attitude dynamics can be divided into two loops: the external loop and the inner loop. In the external loop, the system output is the attitude angle, such as the pitch, yaw, and roll angles for each channel, and the attitude angular velocity is taken as the control input. In the inner loop, the attitude angular velocity and control torque are regarded as the system output and control input, respectively.

For the external loop, in order to track the desired attitude angle, the objective function is given by

$$J_1(x_2(k)) = |x_1^*(k+1) - x_1(k+1)|^2, \tag{15}$$

where $x_1^*(k+1)$ is the desired attitude angle at $k+1$.

Differentiating the objective function with respect to $x_2(k)$ and letting it be equal to zero, one may obtain

$$x_{2d}(k) = \frac{x_1^*(k+1) - x_1(k)}{T}, \tag{16}$$

where $x_{2d}(k)$ is the desired signal of $x_2$ generated by the external loop.

For the inner loop controller design, the following objective function is considered:

$$J_2(u(k)) = \left| \frac{x_{2d}(k+1) + x_2^*(k+1)}{2} - x_2(k+1) \right|^2 + \lambda |u(k)|^2, \tag{17}$$

where $x_2^*(k+1)$ is the reference attitude angular velocity and $\lambda > 0$.

By minimizing the objective function (17) with respect to $u(k)$ and introducing the step-size parameters, one can obtain the following modified adaptive control law

$$u(k) = \frac{\rho_1 \phi(k)(x_{2d}(k+1) - x_2(k)) + \rho_2 \phi(k)(x_2^*(k+1) - x_2(k))}{\lambda + |\phi(k)|^2}, \tag{18}$$

where $\rho_1 \in (0,1)$, $\rho_2 \in (0,1)$.

Considering the limited capacity of the actuator, the input of the controlled system is constrained by

$$|u(k)| \leq \kappa, \tag{19}$$

where $\kappa$ is the maximum value of the control input and $\kappa > 0$.

Note that the exact value of PPD parameter $\phi(k)$ in control law (18) is unknown and difficult to obtain. Thus, to estimate the value of $\phi(k)$, the following cost function is employed:

$$J(\hat{\phi}(k)) = \left| x_2(k) - x_2(k-1) - \hat{\phi}(k)u(k-1) \right|^2 + \mu \left| \hat{\phi}(k) - \hat{\phi}(k-1) \right|^2, \tag{20}$$

where $\hat{\phi}(k)$ is the estimated variable of $\phi(k)$ and $\mu > 0$.

By minimizing Equation (20) with respect to $\hat{\phi}(k)$, the following PPD estimation algorithm is obtained:

$$\hat{\phi}(k) = \hat{\phi}(k-1) + \frac{\eta u(k-1)\big(x_2(k) - x_2(k-1) - \hat{\phi}(k-1)u(k-1)\big)}{\mu + |u(k-1)|^2}, \tag{21}$$

where $\eta \in (0, 1]$ is a step-size factor.

Combining the above algorithm, the modified model-free adaptive control (MMFAC) scheme can be described as follows

$$\hat{\phi}(k) = \hat{\phi}(k-1) + \frac{\eta u(k-1)\big(x_2(k) - x_2(k-1) - \hat{\phi}(k-1)u(k-1)\big)}{\mu + |u(k-1)|^2}, \tag{22}$$

$$\hat{\phi}(k) = \hat{\phi}(1), \text{ if } \hat{\phi}(k) \leq \varepsilon, \tag{23}$$

$$u(k) = \begin{cases} \frac{\rho_1 \hat{\phi}(k)(x_{2d}(k+1) - x_2(k)) + \rho_2 \hat{\phi}(k)\left(x_2^*(k+1) - x_2(k)\right)}{\lambda + \left|\hat{\phi}(k)\right|^2}, & for |u(k)| \leq \kappa, \\ \kappa sign(u(k)), & for |u(k)| \geq \kappa, \end{cases} \tag{24}$$

where $\varepsilon$ is a very small positive constant, and $\hat{\phi}(1)$ is the initial value of $\hat{\phi}(k)$. The reset algorithm (23) is proposed to limit the amount of control input and ensure that the PPD parameter is bounded.

**Remark 2.** *The objective function (17) consists of two purposes, namely, to minimize the tracking error of $x_2(k+1)$ and the control input consumption of $u(k)$. It is noted that for the calculation of the tracking error of $x_2(k+1)$, the reference signal is defined as the mean value of $x_{2d}(k+1)$ and $x_2^*(k+1)$. The aim of designing such objective function is to track the reference signals $x_{2d}(k+1)$ and $x_2^*(k+1)$ accordingly, with the consideration of minimizing the attitude angle and attitude velocity tracking errors. The proof for this problem is presented in Section 3.2.*

**Remark 3.** *In order to improve the effectiveness and robustness of the MFAC controller, some researchers have introduced a damping effect into the controller, as seen in the PD-MFAC controller [21] and the improved MFAC method [29]. However, adding damping to the controller is an indirect approach, to some extent, and may result in slowing down the speed of convergence. In contrast, the proposed MMFAC method takes a more direct approach. By reestablishing a two-loop data model that specifically accounts for the vehicles attitude angle and attitude angular velocity and designing the preferable performance index and cost function, the MMFAC method can more accurately capture the dynamic characteristics of the morphing vehicles. As a result, the proposed MMFAC controller would exhibit more efficient attitude tracking performance and robustness.*

#### 3.1.2. Actuator Control Strategy Design

Note that the control input $u(k)$ of the MMFAC scheme represents the control torque, and the signal of the control torque needs to be transformed into a signal of the rudder deflection angle by interpolating the pneumatic database in practice. However, the aerodynamic data of the controlled vehicle is unknown, as the aerodynamic model has not been established during the design of the data-driven controller. To overcome this difficulty, the original CFDL-MFAC algorithm is employed to establish the dynamic data model of the rudder actuator and the design a controller to track the reference signal of control torque generated by the attitude controller.

Since the change in the control torque $\Delta M$ (system output) with regard to the change in the rudder deflection angle $\Delta\delta$ (control input) is approximately monotonic, satisfying the conditions of MFAC theory, one can obtain the following data model for the control torque and rudder deflection angle:

$$\Delta e_M(k+1) = \phi_c \Delta\delta(k) \tag{25}$$

where $\Delta e_M(k+1)$ is the change in the tracking error of the control torque $e_M(k+1) = M_d(k+1) - M(k+1)$ where $M_d(k+1)$ is the desired control torque generated by the control law (24), and $\Delta\delta(k) = \delta(k) - \delta(k-1)$ represents the change of the actual rudder deflection angle $\delta(k)$ and $|\phi_c(k)| < \overline{b}$.

According to the error model (25) and the CFDL-MFAC algorithm, the following control scheme can be obtained:

$$\hat{\phi}_c(k) = \hat{\phi}_c(k-1) + \frac{\eta_2 \Delta\delta(k-1)}{\mu_2 + |\Delta\delta(k-1)|^2}\left(\Delta e_M(k) - \hat{\phi}_c(k-1)\Delta\delta(k-1)\right), \tag{26}$$

$$\hat{\phi}_c(k) = \hat{\phi}_c(1),\ if\left|\hat{\phi}_c(k)\right| \le \varepsilon\ or\ sign\left(\hat{\phi}_c(k)\right) \ne sign\left(\hat{\phi}_c(1)\right), \tag{27}$$

$$\delta(k) = \delta(k-1) + \frac{\rho_3 \hat{\phi}_c(k)}{\lambda_2 + \left|\hat{\phi}_c(k)\right|^2}(0 - e_M(k)), \tag{28}$$

where $\mu_2 > 0, 0 < \eta_2 < 1, \varepsilon > 0, 0 < \rho_3 < 1$ and $\lambda_2 > 0$.

**Remark 4.** *With the assumption that positive rudder surface deflection produces negative control torque, it is implied that the tracking error $e_M$ with regard to the change of the rudder deflection angle $\Delta\delta$ is a negative correlation. Thus, as seen from the control law (28), the sign of $\hat{\phi}_c(k)$ must be positive for each moment.*

### *3.2. Stability Analysis*

The stability analysis comprises three steps. First, we aim to demonstrate the boundedness of the estimated error of PPD, ensuring its convergence within acceptable limits. In the second step, the proof of the boundedness of the attitude error under the control of the proposed MMFAC method is presented. This analysis is performed to validate the control method's effectiveness in maintaining attitude stability and accurate attitude tracking. Finally, the third step aims to verify the convergence of the control torque tracking error when the rudder deflection actuator is regulated by the proposed actuator controller. This proof assures the controller's ability to achieve precise control torque tracking, further ensuring overall system stability.

**Theorem 1.** *Under Assumption 3, based on the estimation law of Equation (22), the estimation error of the PPD parameter is uniformly ultimately bounded (UUB).*

**Proof.** Define the estimation error as $\widetilde{\phi}(k) = \hat{\phi}(k) - \phi(k)$. Subtracting $\phi(k)$ from both sides of Equation (22) leads to

$$\begin{aligned}\widetilde{\phi}(k) &= \hat{\phi}(k-1) - \phi(k) + \frac{\eta u(k-1)\left(x_2(k) - x_2(k-1) - \hat{\phi}(k-1)u(k-1)\right)}{\mu + |u(k-1)|^2} \\ &= \hat{\phi}(k-1) - \phi(k-1) + \frac{\eta|u(k-1)|^2\left(\phi(k-1) - \hat{\phi}(k-1)\right)}{\mu + |u(k-1)|^2} + \phi(k-1) - \phi(k)\ . \\ &= \left(1 - \frac{\eta|u(k-1)|^2}{\mu + |u(k-1)|^2}\right)\widetilde{\phi}(k-1) + \phi(k-1) - \phi(k)\end{aligned} \tag{29}$$

Taking the absolute value on the both sides of Equation (29), one obtains

$$\left|\widetilde{\phi}(k)\right| \le \left|1 - \frac{\eta|u(k-1)|^2}{\mu + |u(k-1)|^2}\right|\left|\widetilde{\phi}(k-1)\right| + |\phi(k-1)| + |\phi(k)|. \tag{30}$$

Since the function $\eta|u(k-1)|^2/\left(\mu + |u(k-1)|^2\right)$ is monotonically increasing with respect to $|u(k-1)|^2$, its minimum value is equal to $\eta\tau^2/\left(\mu + \tau^2\right)$ when $|u(k-1)| \ge \tau$,

with $\tau$ being a positive constant. With $\eta \in (0,1]$ and $\mu > 0$, the following inequality can be obtained:

$$\left|1 - \frac{\eta |u(k-1)|^2}{\mu + |u(k-1)|^2}\right| \leq 1 - \frac{\eta \tau^2}{\mu + \tau^2} \triangleq d_1 < 1. \tag{31}$$

According to $0 < \phi(k) \leq b$ and the above analysis, one can obtain the following inequality from Equation (30):

$$\begin{array}{ll} |\widetilde{\phi}(k)| & \leq d_1 |\widetilde{\phi}(k-1)| + 2b \\ & \leq {d_1}^2 |\widetilde{\phi}(k-2)| + 2d_1 b \\ & \vdots \\ & \leq {d_1}^{k-1} |\widetilde{\phi}(1)| + \frac{2b\left(1-{d_1}^{k-1}\right)}{1-d_1} \end{array}. \tag{32}$$

Seen from Equations (30)–(32), when $|u(k-1)| \geq \tau$, $\widetilde{\phi}(k)$ is uniformly bounded. Additionally, the estimation of PPD $\hat{\phi}(k)$ is bounded due to the fact that $\phi(k)$ is bounded. When $u(k) = 0$, one can obtain $\hat{\phi}(k+1) = \hat{\phi}(k)$ from the estimation algorithm, which implies that $\hat{\phi}(k+1)$ is bounded as well. □

**Theorem 2.** *By using the MMFAC law (24), the attitude angle tracking error $e_1(k) = x_1^*(k) - x_1(k)$ and the attitude angular velocity tracking error $e_2(k) = x_2^*(k) - x_2(k)$ are UUB for all time momentk. When the reference signals are time-varying, the tracking errors are limited with the ultimate bound $\lim_{k\to\infty} |e_1(k)| \leq Td_2\varsigma/(1-d_2)$ and $\lim_{k\to\infty} |e_2(k)| \leq d_2\varsigma/(1-d_2)$, respectively. When the reference signals are invariant constants, the tracking errors converge to zero, namely, $\lim_{k\to\infty} |e_1(k)| = \lim_{k\to\infty} |e_2(k)| = 0$.*

**Proof.** The control law (24) can be equivalently written as

$$u(k) = s(k)\frac{\rho_1 \phi(k)(x_{2d}(k+1) - x_2(k)) + \rho_2 \phi(k)(x_{2r}(k+1) - x_2(k))}{\lambda + |\phi(k)|^2} \tag{33}$$

where

$$s(k) = \begin{cases} 1, & \text{for } |u(k)| \leq \kappa \\ \frac{\kappa}{|u(k)|}, & \text{for } |u(k)| > \kappa \end{cases},$$

which implies that $0 < s(k) \leq 1$.

Define the tracking error as follows:

$$e_3(k+1) = x_{2d}(k+1) - x_2(k+1), \tag{34}$$

According to the data model (13) and control law (33), one can obtain the following equality:

$$\begin{array}{ll} & e_3(k+1) + e_2(k+1) \\ = & x_{2d}(k+1) - x_2(k) + x_{2r}(k+1) - x_2(k) \\ & -2\rho_1 \xi(k)(x_{2d}(k+1) - x_2(k)) - 2\rho_2 \xi(k)(x_{2r}(k+1) - x_2(k)) \\ = & (1 - 2\rho_1 \xi(k))(x_{2d}(k+1) - x_2(k)) + (1 - 2\rho_2 \xi(k))(x_{2r}(k+1) - x_2(k)) \\ = & (1 - 2\rho_1 \xi(k))(e_3(k) + \Delta x_{2d}(k+1)) + (1 - 2\rho_2 \xi(k))(e_2(k) + \Delta x_{2r}(k+1)) \end{array}, \tag{35}$$

where $\xi(k) = \left(s(k)\phi(k)\hat{\phi}(k)\right) / \left(\lambda + \left|\hat{\phi}(k)\right|^2\right)$, $\Delta x_{2d}(k+1) = x_{2d}(k+1) - x_{2d}(k)$, $\Delta x_{2r}(k+1) = x_{2r}(k+1) - x_{2r}(k)$.

Since $\rho_1 \in (0,1)$, $s(k) \in (0,1]$, $0 < \phi(k) \leq b$ and $\lambda \geq b^2$, one has

$$0 < \rho_1 \xi(k) \leq \rho_1 s(k) \frac{b\hat{\phi}(k)}{\lambda + \left|\hat{\phi}(k)\right|^2} \leq \rho_1 s(k) \frac{b\hat{\phi}(k)}{2b\hat{\phi}(k)} < \frac{1}{2}. \tag{36}$$

Similar to the above process, one can obtain $0 < \rho_2\xi(k) < 1/2$, thus yielding $0 < 1 - 2\rho_1\xi(k) < 1$ and $0 < 1 - 2\rho_2\xi(k) < 1$. Taking the absolute value on the both sides of Equation (35), the following inequality can be obtained:

$$|e_3(k+1)| + |e_2(k+1)| \leq d_2(|e_3(k)| + |e_2(k)|) + d_2 a_1 \tag{37}$$

where $d_2 = \max\{1 - 2\rho_1\xi(k), 1 - 2\rho_2\xi(k)\}$, $a_1(k+1) = |\Delta x_{2d}(k+1)| + |\Delta x_{2r}(k+1)|$. It is known that the desired trajectory is continuous and cannot change rapidly in practice, so the change of the desired state is bounded. Thus, by assuming that $a_1(k) \leq \varsigma$ where $\varsigma > 0$ is a constant, one can obtain

$$\begin{aligned} |e_3(k+1) + e_2(k+1)| &\leq d_2|e_3(k) + e_2(k)| + d_2\varsigma \\ &\leq d_2^2|e_3(k-1) + e_2(k-1)| + d_2^2\varsigma + d_2\varsigma \\ &\vdots \\ &\leq d_2^k|e_3(1) + e_2(1)| + \tfrac{d_2\varsigma\left(1-d_2^k\right)}{1-d_2} \end{aligned} \tag{38}$$

which implies that the sum of the tracking errors is uniformly ultimately bounded UUB for all k with ultimate bound $\lim_{k\to\infty}(|e_3(k)| + |e_2(k)|) \leq d_2\varsigma/(1-d_2)$. Hence, one can easily see that $\lim_{k\to\infty}|e_2(k)| \leq d_2\varsigma/(1-d_2)$ and $\lim_{k\to\infty}|e_3(k)| \leq d_2\varsigma/(1-d_2)$.

Notice that

$$\begin{aligned} e_1(k+1) &= x_1^*(k+1) - x_1(k+1) \\ &= T\left(\tfrac{x_1^*(k+1)-x_1(k)}{T} - x_2(k)\right) \\ &= Te_3(k) \end{aligned} \tag{39}$$

Therefore, one obtains $\lim_{k\to\infty}|e_1(k)| \leq T\lim_{k\to\infty}|e_3(k)| \leq Td_2\varsigma/(1-d_2)$.

Furthermore, when the reference signals $x_1^*(k)$ and $x_2^*$ are invariant constants, one can acquire $\varsigma = 0$. From the above results, $\lim_{k\to\infty}|e_1(k)| = 0$ and $\lim_{k\to\infty}|e_2(k)| = 0$ can be obtained. □

**Theorem 3.** *The actual control torques generated by the actuator can converge to the reference value monotonically by using the CFDL-MFAC scheme (26)~(28) when* $\lambda_2 > \frac{\overline{b}^2}{4}$.

**Proof.** The error model (25) and control law (28) yield

$$|e_M(k+1)| = |e_M(k) + \phi_c(k)\Delta\delta(k)| \leq \left|1 - \frac{\rho_3\phi_c(k)\hat{\phi}_c(k)}{\lambda_2 + \left|\hat{\phi}_c(k)\right|^2}\right||e_M(k)|. \tag{40}$$

Since $0 < \rho_3 < 1$, $\underline{\varepsilon} < \phi_c(k) < \overline{b}$ and $\lambda_2 > \frac{\overline{b}^2}{4}$, one can obtain

$$0 < \frac{\rho_3\phi_c(k)\hat{\phi}_c(k)}{\lambda_2 + \left|\hat{\phi}_c(k)\right|^2} < \frac{\overline{b}\hat{\phi}_c(k)}{\lambda_2 + \left|\hat{\phi}_c(k)\right|^2} < 1 \tag{41}$$

Thus,

$$0 \leq \left|1 - \frac{\rho_3\phi_c(k)\hat{\phi}_c(k)}{\lambda_2 + \left|\hat{\phi}_c(k)\right|^2}\right| \triangleq d_3 \leq 1 \tag{42}$$

Consequently, the control algorithm (26)~(28) can ensure the convergence of the tracking error to zero, since $\lim_{k\to\infty}|e_M(k+1)| \leq \lim_{k\to\infty}{d_3}^k|e_M(1)| = 0$. □

## 4. Simulations and Results

In this section, simulations for the large-scale morphing unmanned vehicle are presented to illustrate the performance of the proposed control scheme. In order to generate

the I/O data, which is necessary for the data-driven controller, a time-varying six-degree-of-freedom (6DOF) dynamics model of a morphing vehicle in [29] is used in the simulations, which is presented in Appendix A.

The initial states of the morphing vehicle are set in Table 2.

**Table 2.** The initial states of the morphing vehicle.

| States | Values | States | Values |
|---|---|---|---|
| $V_0$ | 3.32 km/s | $\varphi_0$ | 5 deg |
| $x_0$ | 0 m | $\psi_0$ | 5 deg |
| $y_0$ | 45 km | $\gamma_0$ | 5 deg |
| $z_0$ | 0 m | $\omega_{x0}$ | 0 deg/s |
| $\alpha_0$ | 2 deg | $\omega_{y0}$ | 0 deg/s |
| $\beta_0$ | 0 deg | $\omega_{z0}$ | 0 deg/s |

In this numerical simulation, the morphing vehicle is supposed to increase its wing span by 50% in 3 s, that is, to rapidly morph from the original state (State I) to another state (State II). With the morphing process, the whole flight of the morphing vehicle is divided into five phases, planned as follows.

Phase A: the morphing vehicle tracks the desired attitude ($\varphi_d = 10$ deg, $\psi_d = 0$ deg, $\gamma_d = 0$ deg) in 10 s while maintaining State I.

Phase B: maintain the stability of the attitude during morphing from State I to State II.

Phase C: track the desired attitude ($\varphi_d = 15$ deg, $\psi_d = 2$ deg, $\gamma_d = 2$ deg) within 10 s in State II.

Phase D: track the desired attitude ($\varphi_d = 10$ deg, $\psi_d = 0$ deg, $\gamma_d = 0$ deg) while morphing from State II to State I.

Phase E: continue tracking the desired attitude in State I.

The states and desired attitude angles of the morphing vehicle at different phases are shown in Figures 3 and 4. Phase A is used to investigate the effectiveness of the proposed controller in initial State I, establishing a baseline for further simulation. In Phase B, the controller's ability to maintain the attitude stabilization is rigorously tested under the large deformations to which the vehicle is subjected, ensuring its robustness in challenging scenarios. Phase C is used to demonstrate the controller's ability to track different attitude angles in different states, highlighting its adaptability to different tasks. Finally, in Phase D, the controller is required to track the desired attitude angles as the vehicle is undergoing large-scale morphing, evaluating the tracking performance of the proposed controller under demanding scenarios.

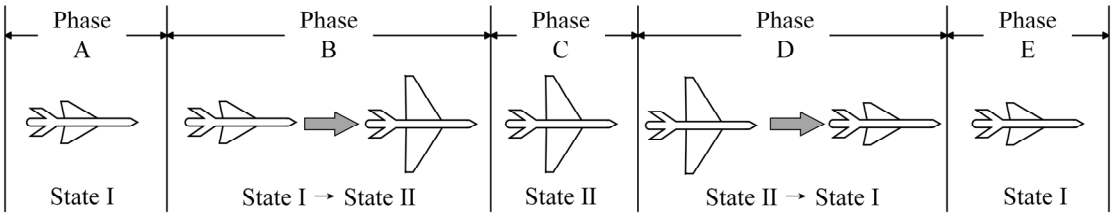


**Figure 3.** The state of the morphing vehicle in five phases.

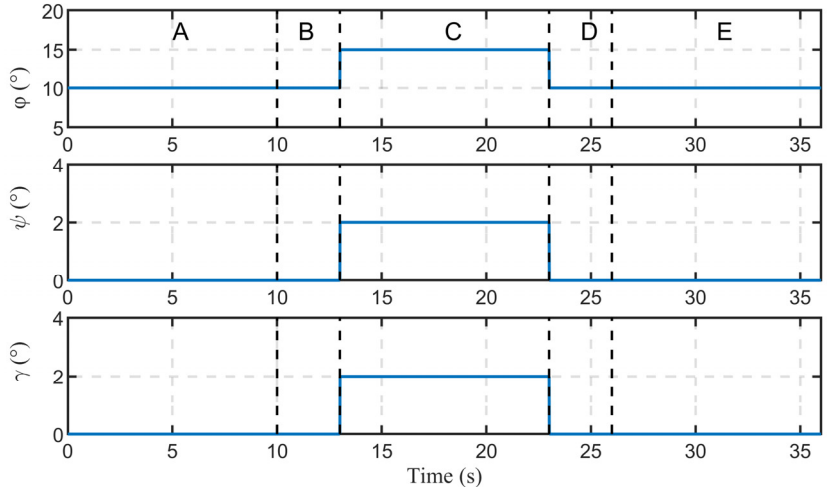


**Figure 4.** The desired attitude angles in different phases.

The parameters of control scheme Equations (22)–(24) are shown in Table 3. The sampling time $T$ is taken as 0.01 s.

**Table 3.** The value of the parameters of MMFAC.

| Method | Parameter | Value | | |
|---|---|---|---|---|
| | | Pitch | Yaw | Roll |
| MMFAC | $\eta$ | 0.01 | 0.05 | 0.05 |
| | $\mu$ | 1 | 1 | 1 |
| | $\rho_1$ | 0.01 | 0.01 | 0.008 |
| | $\rho_2$ | 0.8 | 0.9 | 0.9 |
| | $\lambda$ | $8 \times 10^{-11}$ | $2 \times 10^{-11}$ | $1 \times 10^{-8}$ |
| | $\hat{\phi}(1)$ | $1 \times 10^{-5}$ | $2 \times 10^{-5}$ | $2 \times 10^{-4}$ |

The parameters of the rudder actuator control algorithm (26)–(28) are shown in Table 4.

**Table 4.** The value of the parameters of the rudder actuator.

| Method | Parameter | Value | | |
|---|---|---|---|---|
| | | Pitch | Yaw | Roll |
| CFDL-MFAC | $\eta_2$ | 0.5 | 0.5 | 0.5 |
| | $\mu_2$ | 1 | 1 | 1 |
| | $\rho_3$ | 0.75 | 0.5 | 0.5 |
| | $\lambda_2$ | 1 | 1 | 1 |
| | $\hat{\phi}_c(1)$ | $3.1 \times 10^3$ | $9.5 \times 10^2$ | $8 \times 10^2$ |

It is difficult to achieve the flight control of the vehicle using the original CFDL-MFAC controller [21]. In order to verify the effectiveness of the proposed controller, the PD-MFAC approach shown in Equation (10) is taken as a baseline controller for performance comparison, and the parameters of PD-MFAC are shown in Table 5.

**Table 5.** The value of the parameters of PD-MFAC.

| Method | Parameter | Value | | |
|---|---|---|---|---|
| | | **Pitch** | **Yaw** | **Roll** |
| PD-MFAC | $\eta_1$ | 0.5 | 0.1 | 0.1 |
| | $\mu_1$ | 1 | 1 | 1 |
| | $\rho$ | 0.4 | 0.9 | 0.9 |
| | $\lambda_1$ | $2 \times 10^{-7}$ | $5 \times 10^{-7}$ | $1 \times 10^{-5}$ |
| | $K_y$ | $5 \times 10^{4}$ | $6.5 \times 10^{4}$ | $9 \times 10^{3}$ |
| | $K_{dy}$ | $6.5 \times 10^{3}$ | $8 \times 10^{3}$ | $8 \times 10^{2}$ |
| | $\hat{\xi}(1)$ | $3.5 \times 10^{-4}$ | $1.8 \times 10^{-3}$ | $1.7 \times 10^{-2}$ |

Considering the maximum control torque that can be provided by the practical actuators, the maximum control input is set as 200 N·m .

Case 1: The disturbances are not considered in this case, i.e., $d_{M_x} = d_{M_y} = d_{M_z} = 0$ in Equation (A2). Simulation results are shown in Figures 5–7. Figure 5 presents the attitude tracking performance in the three channels of MMFAC and PD-MFAC. It can be seen that both controllers can successfully track the desired attitude angles before, during, and after morphing, corresponding to Phase A, D, and C, respectively. However, the MMFAC achieves a faster tracking response than does the PD-MFAC. As shown in Figures 6 and 7, the PD-MFAC controller leads to high-amplitude and oscillatory control torques and rudder deflections due to the employment of the damping term in the controller, while the MMFAC controller results in smooth control torques and rudder deflections due to the use of the novel data model, as demonstrated in Remark 3 in Section 3. A. Further, taking the pitch channel as an example, the controller (24) includes $\varphi(k)$ and $\dot{\varphi}(k)$, while the PD-MFAC controller (10) includes $\varphi(k)$, $\Delta\varphi(k)$ and $\Delta\varphi(k-1)$, which implies that the proposed controller achieves greater performance with less feedback information and validates the superiority of the developed data model in Equation (13).

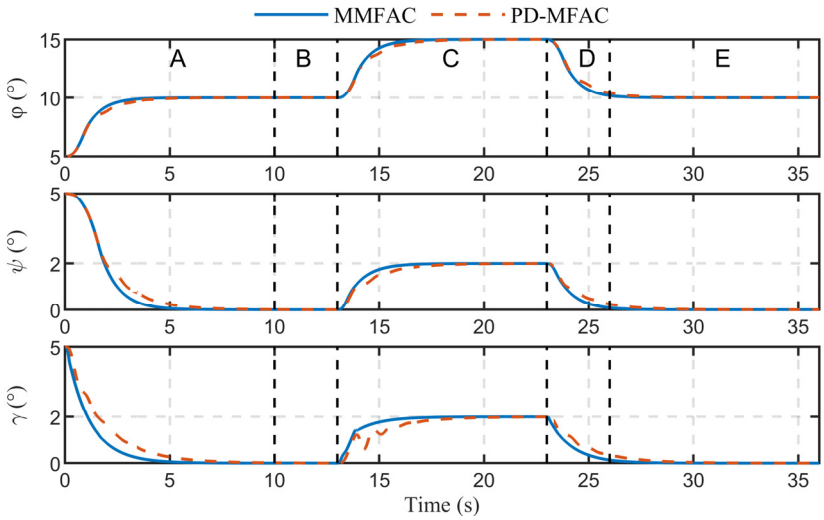


**Figure 5.** Tracking performance in the absence of disturbances.

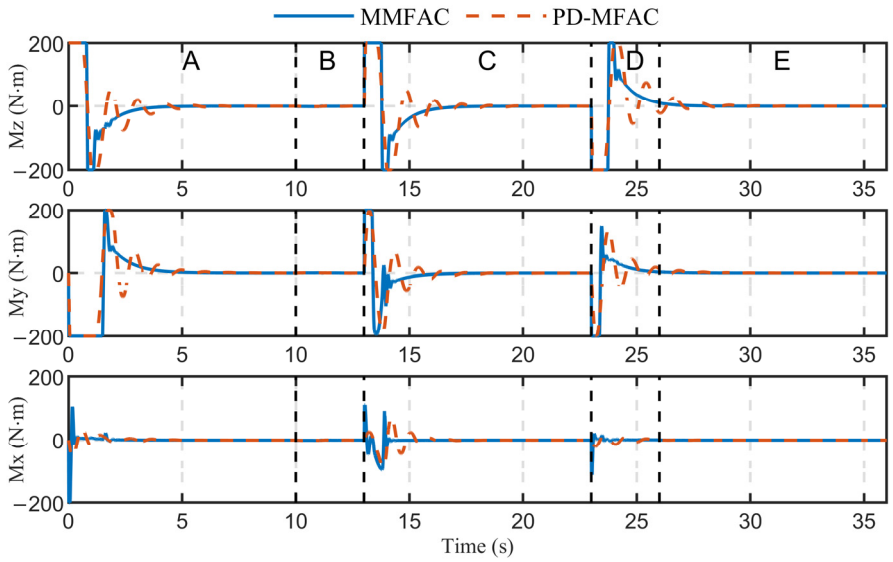


**Figure 6.** Time histories of control torque in the absence of disturbances.

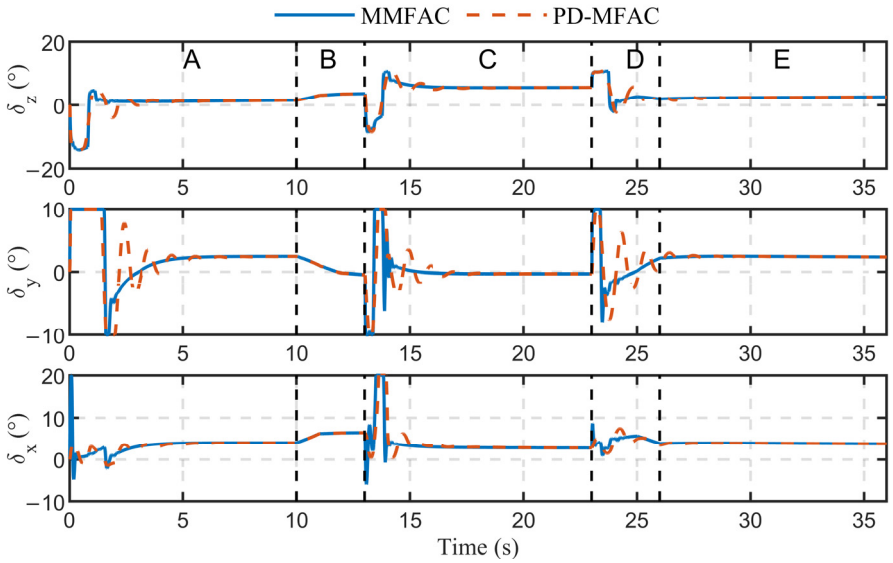


**Figure 7.** Time histories of rudder deflection in the absence of disturbances.

Case 2: The disturbances $d_{M_x}$, $d_{M_y}$, and $d_{M_z}$ in Equation (A2) are set as Equation (43) and, in this subsection, are applied to the morphing unmanned vehicle to investigate the robustness of the proposed controller and PD-MFAC. The responses of the attitudes controlled by the MMFAC and PD-MFAC are shown in Figure 8. It is clear that both controllers succeed in tracking and maintaining the desired attitude in the presence of disturbances, whereas the MMFAC has the advantage of fast convergence. The control torques and the corresponding rudder deflection angles for three channels are shown in Figures 9 and 10. It can be observed that both controllers have the ability to reject disturbances, while the curves of the control input generated by MMFAC are smoother.

$$\begin{cases} d_{M_x} = 1.5(1 + \sin(\frac{\pi}{2}t)) \\ d_{M_y} = 10(1 + \sin(\frac{\pi}{2}t)) \\ d_{M_z} = 10(1 + \sin(\frac{\pi}{2}t)) \end{cases} \tag{43}$$

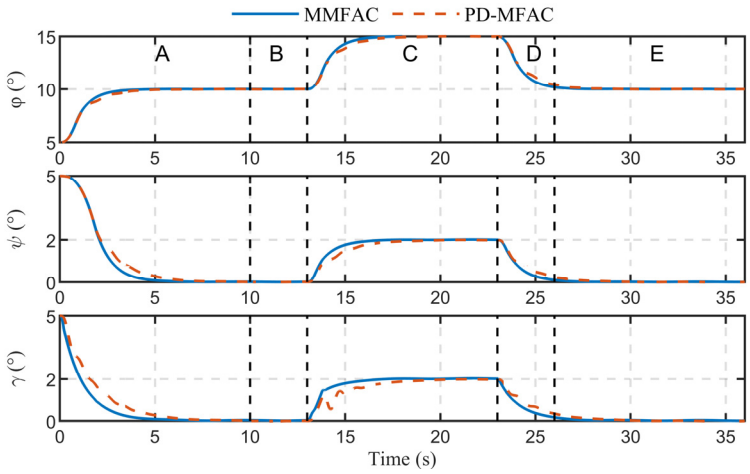


**Figure 8.** Tracking performance in the presence of disturbances.

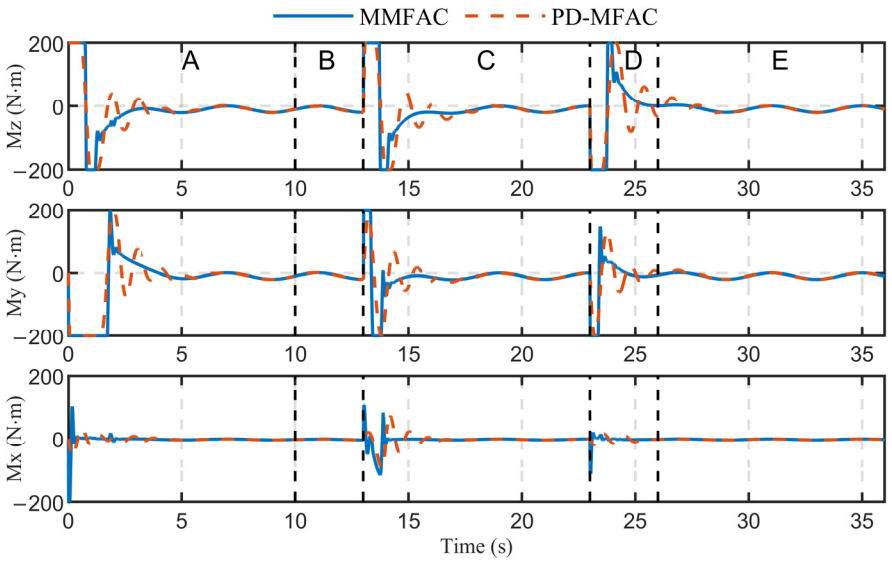


**Figure 9.** Time histories of control torque in the presence of disturbances.

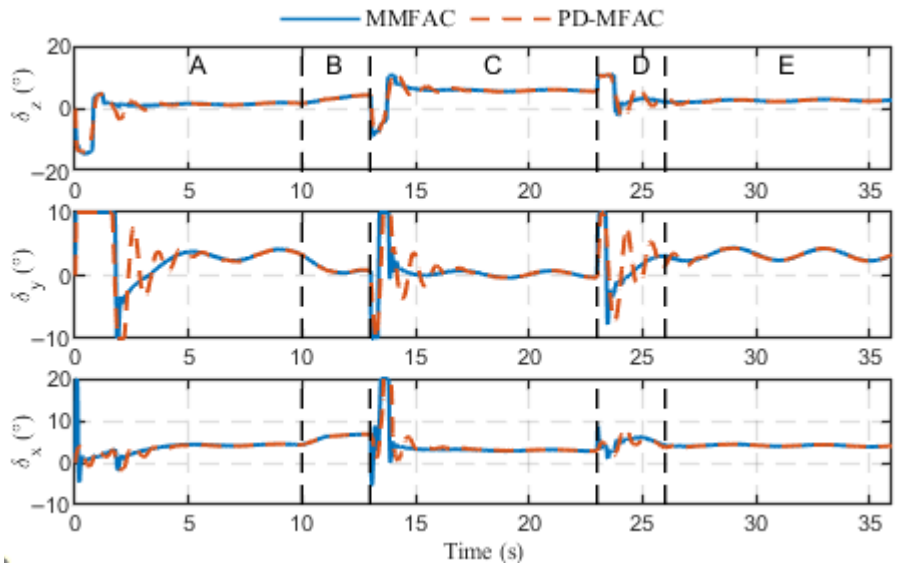


**Figure 10.** Time histories of rudder deflection in the presence of disturbances.

To quantitatively analyze the attitude tracking performance and robustness between the MMFAC and PD-MFAC, the following performance indices are employed [32,33].

(1) Average squared error (*ASE*):

$$\mu_{ASE} = \frac{1}{N}\sum_{i=1}^{N}\Big(\varphi_e^2(i) + \psi_e^2(i) + \gamma_e^2(i)\Big), \tag{44}$$

where $\varphi_e$, $\psi_e$, and $\gamma_e$ are the error of pitch angle, yaw angle, and roll angle, respectively; $N$ is the total step of the simulation. A smaller value of the *ASE* index indicates that the convergent rate of the controller is faster.

(2) Average time-weighted absolute error (*ATAE*):

$$\mu_{ATAE} = \frac{1}{N}\sum_{i=1}^{N}(i|\varphi_e(i)| + i|\psi_e(i)| + i|\gamma_e(i)|). \tag{45}$$

*ATAE* introduces the time-weight into the performance index to focus on analyzing the steady-state error. The smaller the value of *ATAE*, the better tracking performance of the controller.

(3) Total energy consumption (*TEC*):

$$\mu_{TEC} = \frac{1}{N}\sum_{i=1}^{N}(|\delta_x(i)| + |\delta_y(i)| + |\delta_z(i)|). \tag{46}$$

The small *TEC* value represents less energy loss.

The statistical results presented in Table 6 provide a comparison of the effectiveness and robustness between the MMFAC and PD-MFAC method through three performance indices. In Case 1, the values of all performance indices of MMFAC are smaller compared to the those using the PD-MFAC method, which implies that the MMFAC method can achieve a faster convergent rate while utilizing less energy. In Case 2, the presence of disturbances leads to larger values of $\mu_{ATAE}$ and $\mu_{TEC}$ compared to those in Case 1. However, the MMFAC method still outperforms the PD-MFAC method by maintaining smaller values for three performance indices. Notably, the smaller value of $\mu_{ATAE}$ indicates that the MMFAC method exhibits a smaller steady-state error when faced with external disturbances. From the above results, we can draw a conclusion that the proposed MMFAC method possesses superior control performance, particularly in terms of faster convergence and stronger robustness.

**Table 6.** The performance of different controllers in two cases.

| Case | Controller | Value | | |
|---|---|---|---|---|
| | | $\mu_{ASE}$ | $\mu_{ATAE}$ | $\mu_{TEC}$ |
| Case 1 | PD-MFAC | 0.0012 | 25.3916 | 0.1740 |
| | MMFAC | 0.0010 | 19.1274 | 0.1709 |
| Case 2 | PD-MFAC | 0.0012 | 27.4523 | 0.1899 |
| | MMFAC | 0.0010 | 21.2048 | 0.1868 |

## 5. Conclusions

Considering the fast time-varying and strong aerodynamic interference caused by large scale morphing, this paper proposed a MMFAC method for attitude control of morphing unmanned vehicles. The main contributions of this paper are summarized as follows:

(1) By discretizing the dynamic equations of vehicles, which characterize the simplest relationship between attitude angle, attitude angular velocity, and control torque, a novel data model is proposed. Based on the proposed data model, the MMFAC algorithms for the external/inner loop are presented, by designing the corresponding tracking performance index and cost function of the double loop.

(2) Considering the unknown aerodynamic data for the rudder actuators, a data model of the aerodynamic torques is presented, and the corresponding control law of the rudder deflection angle is proposed, which can save a significant amount of effort in establishing the exact aerodynamic model of a morphing unmanned vehicle in contrast to the methods proposed in the earlier work [10].

(3) The convergence of the proposed algorithm has been proved by rigorous mathematical analysis, which shows that the proposed method can ensure the convergence of the tracking error to zero when the reference attitude angle is invariant and guarantee that the tracking errors are uniformly ultimately bounded when tracking a time-varying reference signal.

(4) Compared with the previous controller PD-MFAC [21], simulation results show that the proposed MMFAC controller requires less feedback information, but exhibits a faster convergence rate and preferable robustness in the presence of external disturbances and large morphing.

The data utilized by the controller in this work is accurate and real-time. In future research, a challenge to be addressed is the attitude control in the present of noise and input delay, which is of great significance for stable flight of the morphing unmanned vehicles in complex missions. In addition, a semi-physical experimental platform will be constructed to demonstrate the validity of the proposed method.

**Author Contributions:** Conceptualization, H.C., J.C., G.B. and J.W.; methodology, H.C. and J.W.; validation, H.C.; resources, G.B.; writing—original draft preparation, H.C.; writing—review and editing, J.W.; funding acquisition, J.C. and G.B. All authors have read and agreed to the published version of the manuscript.

**Funding:** This research was funded by the National Natural Science Foundation of China (Grant number 62103452).

**Data Availability Statement:** Some or all data, models, or code that support the findings of this study are available from the corresponding author upon reasonable request.

**Acknowledgments:** This work was supported by the National Natural Science Foundation of China (Grant numbers 62103452).

**Conflicts of Interest:** The authors declare no conflict of interest.

## Appendix A

The 6-DOF dynamic equations of the morphing unmanned vehicle used in the simulation are presented as follows:

$$\begin{cases} \dot{V} = & \frac{C_Z qS - mg\sin\varphi\sin\psi\cos\gamma + mg\cos\varphi\sin\gamma}{m}\sin\beta \\ & + \frac{-C_A qS - mg\sin\varphi\cos\psi}{m}\cos\alpha\cos\beta \\ & - \frac{C_N qS - mg\cos\varphi\cos\gamma - mg\sin\varphi\sin\psi\sin\gamma}{m}\sin\alpha\cos\beta \\ \dot{\alpha} = & \omega_{z1} + \frac{\sin\alpha\sin\beta}{\cos\beta}\omega_{y1} - \frac{\cos\alpha\sin\beta}{\cos\beta}\omega_{x1} \\ & - \frac{(C_N qS - mg\cos\varphi\cos\gamma - mg\sin\varphi\sin\psi\sin\gamma)\cos\alpha}{mV\cos\beta} \\ & - \frac{(-C_A qS - mg\sin\varphi\cos\psi)\sin\alpha}{mV\cos\beta} \\ \dot{\beta} = & \omega_{y1}\cos\alpha + \omega_{x1}\sin\alpha - \frac{-C_A qS - mg\sin\varphi\cos\psi}{mV}\cos\alpha\sin\beta \\ & + \frac{C_N qS - mg\cos\varphi\cos\gamma - mg\sin\varphi\sin\psi\sin\gamma}{mV}\sin\alpha\sin\beta \\ & + \frac{C_Z qS - mg\sin\varphi\sin\psi\cos\gamma + mg\cos\varphi\sin\gamma}{mV}\cos\beta \\ \dot{X} = & V\cos\theta\cos\sigma \\ \dot{Y} = & V\sin\theta\cos\sigma \\ \dot{Z} = & -V\sin\sigma \\ \dot{\omega}_{x1} = & \frac{M_x - \left(J_z - J_y\right)\omega_{z1}\omega_{y1}}{J_x} \\ \dot{\omega}_{y1} = & \frac{M_y - (J_x - J_z)\omega_{x1}\omega_{z1}}{J_y} \\ \dot{\omega}_{z1} = & \frac{M_z - \left(J_y - J_x\right)\omega_{x1}\omega_{y1}}{J_z} \\ \dot{\gamma} = & \omega_{x1} + \sin\gamma\tan\psi\omega_{y1} + \cos\gamma\tan\psi\omega_{z1} \\ \dot{\psi} = & \cos\gamma\omega_{y1} - \sin\gamma\omega_{z1} \\ \dot{\varphi} = & \frac{\sin\gamma}{\cos\psi}\omega_{y1} + \frac{\cos\gamma}{\cos\psi}\omega_{z1} \\ \sin\sigma = & \cos\alpha\cos\beta\sin\psi + \sin\alpha\cos\beta\cos\psi\sin\gamma - \sin\beta\cos\psi\cos\gamma \\ \sin\theta = & \frac{\cos\alpha\cos\beta\sin\varphi\cos\psi - \sin\alpha\cos\beta(\sin\varphi\sin\psi\sin\gamma + \cos\varphi\cos\gamma)}{\cos\sigma} \\ + & \frac{\sin\beta(\sin\varphi\sin\psi\cos\gamma - \cos\varphi\sin\gamma)}{\cos\sigma} \\ \sin v = & \frac{-\sin\psi\sin\alpha + \cos\alpha\cos\psi\sin\gamma}{\cos\sigma} \end{cases} \tag{A1}$$

where $\alpha$ is the angle of attack, $\beta$ is sideslip angle, $\varphi$ is pitch angle, $\psi$ is yaw angle, and $\gamma$ is roll angle; $C_A$, $C_N$, and $C_Z$ represent the axial fore coefficient, normal force coefficient, and lateral force coefficient, respectively; $q = \rho V^2/2$ is the dynamic pressure, with $\rho$ being the atmospheric density; $S$ is the aerodynamic reference area; $m$ is the total mass of the vehicle; $g$ is the acceleration of gravity; and $V$ is velocity; $\omega_{x1}$, $\omega_{y1}$, and $\omega_{z1}$ are the axis apparent angular velocity in the $ox_1y_1z_1$; $M_x$, $M_y$, and $M_z$ are the control torques in the three channels; $X$, $Y$, and $Z$ are the components of the vehicle position in the launching coordinate system; and $\theta$ is the flight path angle, $\sigma$ is the heading angle, and $v$ is the bank angle.

$$\begin{cases} M_x = C_l qSL + d_{M_x} \\ M_y = C_n qSL + d_{M_y} \\ M_z = C_m qSL + d_{M_z} \end{cases} \tag{A2}$$

where $C_l$, $C_n$, and $C_m$ represent the rolling moment coefficient, yawing moment coefficient, and pitching moment coefficient, respectively; $L$ is the reference length; and $d_{M_x}$, $d_{M_y}$, and $d_{M_z}$ represent the disturbing torque in the roll, yaw, and pitch channel, respectively.

**Remark A1.** *The dynamical equation for the morphing vehicle in Equation (A1) is different from that of the rigid vehicle due to the change in the shape caused by morphing. Furthermore, the change in the shape would directly influence the aerodynamic coefficients, causing the 6-DOF dynamics model to be time-varying. For instance, as the vehicle undergoes morphing, the moment coefficients ($C_l$, $C_n$, and $C_m$) may vary, lending to dynamic changes in the flight behavior of the vehicle.*

## References


1. Siefert, E.; Reyssat, E.; Bico, J.; Roman, B. Bio-inspired pneumatic shape-morphing elastomers. *Nat. Mater.* **2019**, *18*, 24–28. [CrossRef] [PubMed]
2. Dayyani, I.; Shaw, A.D.; Flores, E.I.S.; Friswell, M.I. The mechanics of composite corrugated structures: A review with applications in morphing aircraft. *Compos. Struct.* **2015**, *133*, 358–380. [CrossRef]
3. Wang, C.; Khodaparast, H.H.; Friswell, M.I.; Shaw, A.D.; Xia, Y.; Walters, P. Development of a morphing wingtip based on compliant structures. *J. Intell. Mater. Syst. Struct.* **2018**, *29*, 3293–3304. [CrossRef]
4. Barbarino, S.; Bilgen, O.; Ajaj, R.M.; Friswell, M.I.; Inman, D.J. A review of morphing aircraft. *J. Intell. Mater. Syst. Struct.* **2011**, *22*, 823–877. [CrossRef]
5. Chu, L.; Li, Q.; Gu, F.; Du, X.; He, Y.; Deng, Y. Design, modeling, and control of morphing aircraft: A review. *Chin. J. Aeronaut.* **2021**, *35*, 220–246. [CrossRef]
6. Xu, D.; Hui, Z.; Liu, Y.; Chen, G. Morphing control of a new bionic morphing UAV with deep reinforcement learning. *Aerosp. Sci. Technol.* **2019**, *92*, 232–243. [CrossRef]
7. Andersen, G.; Cowan, D.; Piatak, D. Aeroelastic modeling, analysis and testing of a morphing wing structure. In Proceedings of the 48th AIAA/ASME/ASCE/AHS/ASC Structures, Structural Dynamics, and Materials Conference, Honolulu, HI, USA, 22–26 April 2007; pp. 1734–1748.
8. Kan, Z.; Li, D.; Shen, T.; Xiang, J.; Zhang, L. Aerodynamic characteristics of morphing wing with flexible leading-edge. *Chin. J. Aeronaut.* **2020**, *33*, 2610–2619. [CrossRef]
9. Rodriguez, A. Morphing aircraft technology survey. In Proceedings of the 45th AIAA Aerospace Sciences Meeting and Exhibit, Reno, NV, USA, 8–11 January 2007; pp. 1258–1273.
10. Xu, W.; Li, Y.; Lv, M.; Pei, B. Modeling and switching adaptive control for nonlinear morphing aircraft considering actuator dynamics. *Aerosp. Sci. Technol.* **2022**, *122*, 107349. [CrossRef]
11. Ataei-Esfahani, A.; Wang, Q. Robust failure compensation for a morphing aircraft model using a probabilistic approach. *IEEE Trans. Control. Syst. Technol.* **2007**, *15*, 324–331. [CrossRef]
12. Baldelli, D.H.; Lee, D.H.; Pena, R.S.S.; Cannon, B. Modeling and control of an aeroelastic morphing vehicle. *J. Guid. Control Dyn.* **2008**, *31*, 1687–1699. [CrossRef]
13. Bao, C.; Wang, P.; Tang, G. Integrated method of guidance, control and morphing for hypersonic morphing vehicle in glide phase. *Chin. J. Aeronaut.* **2021**, *34*, 535–553. [CrossRef]
14. Liu, C.; Zhang, S. Novel robust control framework for morphing aircraft. *J. Syst. Eng. Electron.* **2013**, *24*, 281–287. [CrossRef]
15. Yan, B.; Dai, P.; Liu, R.; Xing, M.; Liu, S. Adaptive super-twisting sliding mode control of variable sweep morphing aircraft. *Aerosp. Sci. Technol.* **2019**, *92*, 198–210. [CrossRef]
16. SEmami, A.; Castaldi, P.; Banazadeh, A. Neural network-based flight control systems: Present and future. *Annu. Rev. Control* **2022**, *53*, 97–137.
17. Xiao, Y.; de Ruiter, A.; Ye, D.; Sun, Z. Attitude coordination control for flexible spacecraft formation flying with guaranteed performance bounds. *IEEE Trans. Aerosp. Electron. Syst.* **2022**, *59*, 1534–1550. [CrossRef]
18. Hou, Z.-S.; Wang, Z. From model-based control to data-driven control: Survey, classification and perspective. *Inf. Sci.* **2013**, *235*, 3–35. [CrossRef]
19. Shi, R.; Peng, J. Design of active disturbance rejection control system for morphing flight dynamics. In Proceedings of the 26th Chinese Control and Decision Conference (2014 CCDC), Changsha, China, 31 May–2 June 2014; pp. 1443–1448.
20. Dong, C.; Liu, C.; Wang, Q.; Gong, L. Switched adaptive active disturbance rejection control of variable structure near space vehicles based on adaptive dynamic programming. *Chin. J. Aeronaut.* **2019**, *32*, 1684–1694. [CrossRef]
21. Qi, P.; Zhao, X. Flight control for very flexible aircraft using model-free adaptive control. *J. Guid. Control Dyn.* **2020**, *43*, 608–619. [CrossRef]
22. Iannelli, A.; Fasel, U.; Smith, R.S. The balanced mode decomposition algorithm for data-driven LPV low-order models of aeroservoelastic systems. *Aerosp. Sci. Technol.* **2021**, *115*, 106821. [CrossRef]
23. Hou, Z.; Jin, S. A novel data-driven control approach for a class of discrete-time nonlinear systems. *IEEE Trans. Control Syst. Technol.* **2011**, *19*, 1549–1558. [CrossRef]
24. Hou, Z.; Xiong, S. On model-free adaptive control and its stability analysis. *IEEE Trans. Autom. Control* **2019**, *64*, 4555–4569. [CrossRef]
25. Ma, Y.S.; Che, W.W.; Deng, C.; Wu, Z.G. Distributed model-free adaptive control for learning nonlinear MASs under DoS attacks. *IEEE Trans. Neural Netw. Learn. Syst.* **2021**, *34*, 1146–1155. [CrossRef]
26. Lu, C.; Zhao, Y.; Men, K.; Tu, L.; Han, Y. Wide-area power system stabiliser based on model-free adaptive control. *IET Control Theory Appl.* **2015**, *9*, 1996–2007. [CrossRef]
27. Hou, Z.; Chi, R.; Gao, H. An overview of dynamic-linearization-based data-driven control and applications. *IEEE Trans. Ind. Electron.* **2017**, *64*, 4076–4090. [CrossRef]
28. Xu, D.; Jiang, B.; Shi, P. A novel model-free adaptive control design for multivariable industrial processes. *IEEE Trans. Ind. Electron.* **2014**, *61*, 6391–6398. [CrossRef]
29. Che, H.; Chen, J.; Wang, Y.; Wang, J.; Luo, Y. Data-driven model-free adaptive attitude control for morphing vehicles. *IET Control Theory Appl.* **2022**, *16*, 1696–1707. [CrossRef]

30. Hou, Z.; Jin, S. *Model Free Adaptive Control: Theory and Applications*; CRC Press: Boca Raton, FL, USA, 2019.
31. Wei, C.; Ju, X.; He, F.; Lu, B. Research on non-stationary control of advanced hypersonic morphing vehicles. In Proceedings of the 21st AIAA International Space Planes and Hypersonics Technologies Conference, Xiamen, China, 6–9 March 2017.
32. Liu, K.; Wang, R.; Wang, X.; Wang, X. Anti-saturation adaptive finite-time neural network based fault-tolerant tracking control for a quadrotor UAV with external disturbances. *Aerosp. Sci. Technol.* **2021**, *115*, 106790. [CrossRef]
33. Liu, K.; Wang, R.; Zheng, S.; Dong, S.; Sun, G. Fixed-time disturbance observer-based robust fault-tolerant tracking control for uncertain quadrotor UAV subject to input delay. *Nonlinear Dyn.* **2022**, *107*, 2363–2390. [CrossRef]